Cell, Vol. 94, 525–536, August 21, 1998, Copyright ©1998 by Cell Press

Crystal Structure of the Hexamerization Domain of N-ethylmaleimide–Sensitive Fusion Protein

Christian U. Lenzen,* Diana Steinmann,*
Sidney W. Whiteheart,† and William I. Weis*‡
*Department of Structural Biology
Stanford University School of Medicine
Stanford, California 94305
†Department of Biochemistry
Chandler Medical Center
University of Kentucky College of Medicine
Lexington, Kentucky 40536

Summary

N-ethylmaleimide–sensitive fusion protein (NSF) is a cytosolic ATPase required for many intracellular vesicle fusion reactions. NSF consists of an amino-terminal region that interacts with other components of the vesicle trafficking machinery, followed by two homologous ATP-binding cassettes, designated D1 and D2, that possess essential ATPase and hexamerization activities, respectively. The crystal structure of D2 bound to Mg^{2+}-AMPPNP has been determined at 1.75 Å resolution. The structure consists of a nucleotide-binding and a helical domain, and it is unexpectedly similar to the first two domains of the clamp-loading subunit δ′ of *E. coli* DNA polymerase III. The structure suggests several regions responsible for coupling of ATP hydrolysis to structural changes in full-length NSF.

Introduction

N-ethylmaleimide–sensitive fusion protein (NSF) is a cytosolic ATPase required for many intercompartmental transport steps in both constituitive and regulated secretion (Rothman, 1994; Woodman, 1997; Burgoyne and Morgan, 1998). NSF was purified based on its ability to restore intercisternal Golgi transport to N-ethylmaleimide–treated membranes (Block et al., 1988), and it was shown to be homologous to the *sec18* gene product required for a number of vesicular transport steps in yeast (Eakle et al., 1988; Wilson et al., 1989; Graham and Emr, 1991). NSF binds to membranes through adaptor proteins called soluble NSF attachment proteins (SNAPs), which in turn bind to integral membrane proteins designated SNAP receptors (SNAREs). NSF, SNAPs, and SNAREs form a complex that is believed to be part of a conserved membrane fusion machinery (Bennett and Scheller, 1994; Rothman, 1994; Südhof, 1995). The SNAP–SNARE complex disassembles upon ATP hydrolysis by NSF (Wilson et al., 1992; Söllner et al., 1993a; Nagiec et al., 1995). Because SNARE proteins appear to be derived from opposing vesicle and target membranes, NSF-driven disassembly was originally proposed to drive the actual membrane fusion process (Söllner et al., 1993a, 1993b). Recent studies, however, suggest that NSF acts before membrane fusion to activate SNAREs for their subsequent role in membrane fusion (Banerjee et al., 1996; Mayer et al., 1996; Mayer and Wickner, 1997; Nichols et al., 1997; Weber et al., 1998). It has also been suggested that NSF is involved in recycling the SNAREs after their participation in membrane fusion (Morgan, 1996; Burgoyne and Morgan, 1998). In this manner, NSF may act as a molecular chaperone, using ATP hydrolysis to induce conformational changes in the SNAREs (Morgan and Burgoyne, 1995).

Sequence analysis and limited proteolysis experiments indicate that NSF consists of an amino-terminal domain (N, 1–205) and two ATP-binding domains (D1, 206–487 and D2, 488–752) (Wilson et al., 1989; Tagaya et al., 1993). The N domain is required for interactions with the SNAPs and SNAREs (Whiteheart et al., 1994). The sequences of D1 and D2 each feature the A motif, which contains the phosphate-binding P loop, and the B motif, consisting of hydrophobic residues and a conserved aspartate, that are found in many nucleotide-binding proteins (Walker et al., 1982). The ATPase activity of D1 is essential for the transport activity of NSF (Whiteheart et al., 1994), with ATP binding required for NSF to bind to the SNAP/SNARE complex, and ATP hydrolysis required for disassembly of the complex (Nagiec et al., 1995; Matveeva et al., 1997). In contrast, D2 binds to ATP, but its ATPase activity is not required for NSF to function in transport assays (Whiteheart et al., 1994). Moreover, D2 by itself displays no significant catalytic activity (Nagiec et al., 1995; Matveeva et al., 1997). However, D2 mediates hexamerization of NSF, which is essential for NSF activity (Whiteheart et al., 1994; Fleming et al., 1998), and hexamerization requires the presence of nucleotide (Hanson et al., 1997).

NSF belongs to a large family of Mg^{2+}-dependent ATPases known as AAA proteins (*A*TPases *a*ssociated with various cellular *a*ctivities) (Beyer, 1997; Patel and Latterich, 1998). AAA proteins are found in many organisms and have diverse functions, from proteolysis to membrane trafficking. Proteins in this family contain one or two copies of a 230–250 amino acid cassette that encompasses the Walker A and B motifs (Patel and Latterich, 1998), but little is known about their precise structure.

As a first step toward understanding NSF function, we have determined the crystal structure at 1.75 Å resolution of the D2 domain bound to the nonhydrolyzable ATP analog 5′-adenyl-imido-triphosphate (AMPPNP) and Mg^{2+}. The structure reveals the fold of the AAA cassette, the determinants of nucleotide binding and hexamerization, and suggests its relationship to the D1 domain in full-length NSF. Analysis of the D2 structure and its relationship to other AAA proteins provides a structural basis for understanding how ATP hydrolysis is coupled to conformational changes in these proteins. The structure also reveals a surprising similarity to the clamp-loading subunit of *E. coli* DNA polymerase III (Guenther et al., 1997), suggesting a close connection between these oligomeric ATPases.

‡To whom correspondence should be addressed.

Table 1. Crystallographic Statics

A. Data Collection

	Native		EMP[a]	
	50–1.75 Å	1.83–1.75 Å	50–2.3 Å	2.4–2.3 Å
R_{merge}[b]	.052	.260	.067	.152
% complete	98.4	91.6	99.6	98.2
% $> 3\sigma_I$	78.0	37.0	87.3	68.1
No. reflections	31,212	3600	26,986	3330
Average redundancy	4.2	1.8	3.0	2.4
R_{ISO}[c]	—	—	0.160	0.203

B. Phasing (MLPHARE)

	Phasing power[d]		
Resolution	Acentric	Centric	Figure of Merit
38.10–12.93	3.68	3.17	0.630
12.93–7.79	3.59	2.85	0.596
7.79–5.57	2.87	2.11	0.571
5.57–4.34	2.04	1.40	0.477
4.34–3.55	1.67	1.20	0.434
3.55–3.01	1.68	1.18	0.412
3.01–2.61	1.63	1.20	0.380
2.61–2.30	1.42	1.04	0.323
38.10–2.30	1.74	1.39	0.398

C. Refinement

R values and Temperature Factors		Model Geometry	
No. reflections in working set	26,935	Bond length rmsd from ideal	.0055 Å
R_{cryst}[e]	.199 (.255)[f]	Bond angles rmsd from ideal	1.3°
R_{free}[e]	.223 (.276)[f]	Ramachandran plot	
		% in most favored regions[g]	92.2
Average B	28.7 Å^2	% in additional allowed regions[g]	7.8
Overall anisotropic B		Main chain bond–related B rmsd	1.5 Å^2
B_{11} ($=B_{22}$)	−2.8 Å^2	Main chain angle–related B rmsd	2.2 Å^2
B_{12}	−1.1 Å^2	Side chain bond–related B rmsd	2.5 Å^2
B_{33}	t5.5 Å^2	Side chain angle–related B rmsd	3.7 Å^2

[a] Friedel mates treated as independent observations for all statistics.
[b] $R_{merge} = \Sigma_h\Sigma_i|I_i(h) - <I(h>)|/\Sigma_h\Sigma_i I_i(h)$, where $I_i(h)$ is the i^{th} measurement and $<I(h)>$ is the weighted mean of all measurements of I(h).
[c] $R_{iso} = \Sigma_h||F_{EMP}(h)|-|F_{native}(h)||/\Sigma_h|F_{native}(h)|$
[d] Phasing power $= <|F_H|>/E$, where $<|F_H|>$ is the rms structure factor amplitude for the heavy atom and E is the estimated lack-of-closure error.
[e] R_{cryst} and $R_{free} = \Sigma_h||F(h)_{obs}|-|F(h)_{calc}||/\Sigma_h|F(h)_{obs}|$ for reflections in the working and test sets, respectively.
[f] Numbers in parentheses are for final shell 1.83–1.75 Å.
[g] As defined in PROCHECK (Laskowski et al., 1993).

Results

Structure Determination

Residues 495–752 of Chinese hamster ovary NSF (numbering according to Wilson et al. [1989]) were expressed in *E. coli* with an N-terminal His_6 tag for purification. Crystals grown in the presence of Mg^{2+} and AMPPNP are in the hexagonal space group P6, with one protomer in the asymmetric unit and the molecular and crystallographic 6-fold axes coincident. The structure was determined by single isomorphous replacement with anomalous scattering (Table 1A and 1B) and by electron density modification methods. The refined model (Table 1C) consists of residues 505–750, one AMPPNP, one Mg^{2+}, and solvent molecules. The first 24 and last 2 residues of the expression construct are not visible and are presumably disordered.

Protomer Structure

The NSF D2 protomer consists of a nucleotide-binding domain (residues 505–676), followed by a helical domain (677–750). The first domain has the shape of a triangular wedge characteristic of many nucleotide-binding proteins, with a central five-stranded parallel β sheet flanked by α helices (Figures 1A, 1B, and 1C). As in other nucleotide-binding proteins that have this structural motif, the bound AMPPNP lies in a crevice at the wide end of the wedge corresponding to the C-terminal edge of the β sheet. The second domain consists of four α helices topped by two short antiparallel β strands. The helical domain lies in close apposition to the nucleotide-binding site and contributes several residues to nucleotide binding (see below).

NSF D2 is remarkably and unexpectedly similar in topology and structure to the first two domains of the

δ′ subunit of *E. coli* DNA polymerase III (Guenther et al., 1997) (Figure 1D). Although δ′ is not a nucleotide-binding protein, it is homologous to the polymerase γ subunit, which is an ATPase required for loading the β subunit onto DNA. The five β strands, the P loop, and the following helix (α2) that form the core of the nucleotide-binding domain of D2 and δ′ superimpose with a root-mean-square deviation (rmsd) of 1.1 Å (50 C_α positions). The nucleotide-binding domain of D2 also resembles the core of mitochondrial F1 ATPase (Abrahams et al., 1994), DNA helicases (Subramanya et al., 1996; Korolev et al., 1997), and RecA (Story et al., 1992); for example, the five-stranded β sheet, P loop, and α2 of D2 superimpose on the equivalent residues in RecA with an rmsd of 1.2 Å (54 C_α positions). The second domain of δ′, although it has only three helices, displays a spatial disposition with respect to the nucleotide binding-like domain similar to that observed in D2. Moreover, two of these helices occupy similar positions to those in the helical domain of D2: α7 and α9 of δ′ correspond roughly to α6 and α8 of D2, respectively.

Nucleotide Binding

The nucleoside-binding site of D2 differs from that seen in other P-loop proteins. The adenine moiety adopts a *syn* conformation with respect to the ribose (Figures 2A and 2B), rather than the *anti* conformation observed in other P-loop proteins (Smith and Rayment, 1996). The ribose retains the typical C2′-*endo* conformation. Ile-515 from the N-terminal loop and Ile-715 at the beginning of helix 8 form a sandwich by packing on either side of the adenine ring (Figures 2B and 2C). Ile-516, in the N-terminal loop, and Leu-560, which immediately follows the conserved P-loop residues, contact the edges of the ring. The side chain of Ala-559 and the aliphatic portion of the Lys-716 side chain form van der Waals contacts with the ribose. In addition to these nonpolar contacts, the exocyclic amine (N6) and N7 of adenine form hydrogen bonds with the main chain carbonyl and amide groups of Ile-516. N1 of adenine also forms a hydrogen bond with a water molecule that is positioned by Trp-518 and the main chain of Ser-555 of the P loop. Residues 513 and 514 of the N-terminal loop also form several hydrogen bonds with the 2′ and 3′-OH groups of the ribose. The observed interactions provide an explanation for why GTP binds poorly to D2 (Matveeva et al., 1997): the main chain carbonyl oxygen of Ile-516 would be incompatible with the exocyclic carbonyl oxygen of guanine, and the exocyclic amine of guanine would sterically clash with the main chain at position 556.

In contrast to the unusual mode of nucleoside binding, the triphosphate-binding portion of D2 is very similar to other proteins containing Walker A and B motifs (Figures 2B and 2C). The P loop (A motif) connects strand β1 to helix α2 and forms several hydrogen bonds with the triphosphate moiety of AMPPNP. The P-loop backbone and the conserved residues Lys-557 and Thr-558 adopt conformations very similar to those observed in other proteins. The side chain of Lys-557 forms hydrogen bonds with β- and γ-phosphate oxygen atoms, and Thr-558 coordinates the Mg^{2+}. The B motif encompasses hydrophobic residues of strand β3 and Asp-611 immediately following the strand. The conserved Asp-611 binds to Thr-558. These interactions are identical to those previously observed in P-loop protein–Mg^{2+} nucleotide triphosphate structures.

AAA proteins contain variants of the "DEAD" box, a modified Walker B motif first identified in RNA and DNA helicases (Linder et al., 1989; Koonin, 1993). The first residue is the conserved aspartate of the B motif, and the glutamate is highly conserved. The second two residues are less well conserved, so we refer to this motif as the DExx box. In NSF D1, the DExx sequence is DEID (residues 328–331), and mutation of Glu-329 to glutamine abolishes the ATPase activity and function of NSF (Whiteheart et al., 1994; Nagiec et al., 1995). The corresponding sequence in D2, residues 611–614, is DDIE. Asp-612 is intimately involved in the binding site, where it positions two water molecules that interact with the γ-phosphate and the Mg^{2+} (Figures 2B and 2C), but mutation of this residue to glutamine has no significant effect on NSF function (Whiteheart et al., 1994; Nagiec et al., 1995), consistent with its minimal catalytic activity.

Virtually all of the contacts between AMPPNP and D2 occur within a single protomer. However, the binding site is close to the hexamer interface (Figure 3), and one residue of an adjacent protomer, Lys-639, interacts directly with a γ-phosphate oxygen of the nucleotide as well as Asp-612 (Figures 2B and 2C). It must be emphasized, however, that Lys-639 is not well ordered; the side chain $2F_o-F_c$ electron density is broken between Cδ and Cϵ at the 1.2 σ contour level, and the density does not return in a simulated annealing omit map. Nonetheless, there is always density near the terminal amine (Nζ). Placing Lys-639 in other conformations produced higher R values and negative peaks in F_o-F_c maps. These observations suggest that Lys-639 is partially occupied in the conformation shown in Figure 2B, and that a water molecule likely occupies the Nζ position in a significant fraction of the molecules. Furthermore, Lys-639 is not conserved in other AAA proteins, including the NSF ortholog Sec18p.

Hexamer Structure

The D2 hexamer has the overall appearance of a pinwheel (Figures 3A, 4A, and 4B), consisting of a regular hexagon formed from the triangular nucleotide-binding domains, and protrusions formed by the helical domains. Ignoring the protrusions, the hexamer is approximately 97 Å wide, but when the helical domain is considered, the molecule is 116 Å wide (Figures 4A and 4B). The thickness also varies from 21 Å to 40 Å (Figure 4C). The inner hole is about 18 Å in diameter. These dimensions agree well with electron microscopic images of NSF and its homolog p97 (Peters et al., 1992; Whiteheart and Kubalek, 1995; Hanson et al., 1997). Studies with full-length, D1-D2, and D2 constructs have led to the conclusion that in the presence of nucleotide, D1 and D2 form 120–130 Å diameter rings that sit on top of one another (Hanson et al., 1997). Along the c axis of the crystal, two adjacent unit cells (total length 80.4 Å) contain two hexamers stacked head-to-tail (Figure 4D). The feet formed by the helical domain interact

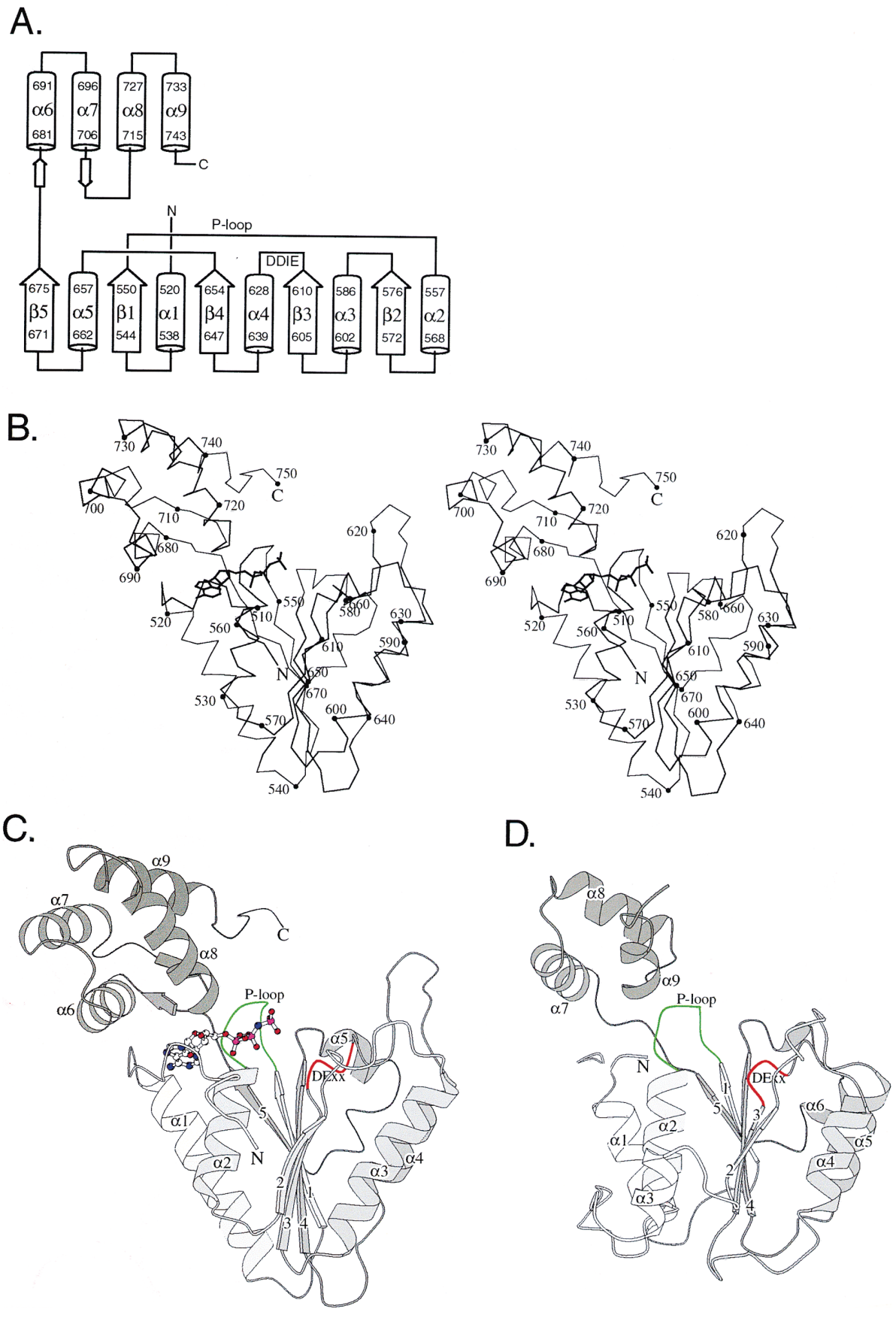

Figure 1. Structure of the NSF D2 Protomer

(A) Topology of D2. Helices are shown as cylinders; strands are shown as as arrows. Residue numbers at the beginning and end of the principal elements of secondary structure are indicated, as well as the locations of the P loop and the DExx box (DDIE in D2). Helices and strands are numbered consecutively in sequence.

(B) Stereo C_α trace of D2. Every tenth C_α is shown as a small sphere and numbered. The bound AMPPNP is shown with thickened black bonds.

with the N terminus of the adjacent hexamer, giving rise to a cavity similar to those seen in images of NSF and in p97. The sequence similary between D1 and D2 indicates that D1 will adopt a structure similar to that described for D2, so it seems likely that the stacking of hexamers in the crystal lattice reflects the organization D1 and D2 in the nucleotide-bound state of NSF.

The triangular shape of the nucleotide-binding domain is exploited in assembling the hexamer, with two of the three sides of the wedge forming interfaces with neighboring protomers (Figure 3). The C-terminal end of α1 and the subsequent turn, and helices 3, 4, 5, and the turns that follow them form one side of the wedge. The other side consists of α8 and the loops between β3 and α4, between β2 and α3, and between β4 and α5. This side also includes part of the ATP-binding site, which is of interest because nucleotide binding appears to stabilize hexameric interactions in NSF: in the absence of nucleotide, D1 is splayed apart from the D2 hexamer ring, and prolonged incubation in the absence of nucleotide dissociates D2 (Hanson et al., 1997). The extended loop between β3 and α4 is especially important as it participates in contacts with both adjacent protomers, forming the inner hole of the hexamer. The interfaces between protomers in the hexamer are extensive and specific. Each protomer buries 2500 Å^2, or approximately 20%, of its solvent-accessible area, upon hexamer formation. The hexamer interface is mixed in character, containing many nonpolar contacts, hydrogen bonds, salt bridges, and water-mediated hydrogen bonds (Figure 3B).

The D2 hexamer displays a polarized charge distribution. The side nearest the N terminus is basic (Figure 4A), whereas the side containing the C terminus is acidic in character (Figure 4B). The location of the N terminus implies that D1 stacks on the basic side of the D2 hexamer. These observations may indicate that electrostatic or polar interactions contribute to the D1-D2 interface. However, a substantial cavity exists between the domains in electron micrographs (Hanson et al., 1997) and between D2 hexamers in the crystal (Figure 4D), such that the electrostatically compatible surfaces may not be in direct contact. Nonetheless, there may be differences in the structure of C-terminal helical domain of D1 with respect to that observed in D2 (see below) that could give rise to more extensive polar interactions between the two domains. The notion that polar interactions mediate the contact between the two ATPase domains is consistent with the large and reversible conformational changes that occur upon loss of nucleotide by D1 (Hanson et al., 1997); a well packed, hydrophobic interface would not be expected to allow a major reorientation of D1 with respect to D2.

Full-length NSF and D2 have recently been shown by a variety of physical methods to be hexameric in solution (Fleming et al., 1998), in contrast to earlier reports which suggested that NSF is a trimer (Whiteheart et al., 1994). The hexamer described here is coincident with the crystallographic 6-fold axis. Space group P6 contains 3-fold and 2-fold rotational symmetry axes parallel to the 6-fold axis, so we considered the contacts between protomers related by these symmetries. Most strikingly, there are no contacts between 3-fold symmetry-related protomers in the lattice. Adjacent hexamers in the lattice pack through the interactions of helices α6 and α7 across a 2-fold axis, in a very small interface compared to that between protomers related by 6-fold rotational symmetry. These observations, along with the agreement of the crystallographic and electron microscopic images of D2, indicate that the hexamer in the crystal represents the oligomeric structure found in solution.

Relationship to Other AAA Domains

An alignment of representative AAA sequences based on the D2 structure is shown in Figure 5. The alignment is based principally on hydrophobic interactions that define the core of the molecule and certain nucleotide-binding residues, and it avoids gaps in regions of regular secondary structure. Although there are almost no invariant residues, the hydrophobic amino acids that form the core of the structure can for the most part be aligned. The five β strands, the first five helices that pack against the β sheet, and residues involved in nucleotide binding are convincingly conserved. Not surprisingly, the sequence identity is best in the conserved P loop, the DExx box, and a stretch of "minimal consensus" residues found in AAA proteins (Patel and Latterich, 1998) that encompass strand 4 and helix 5. Certain elements of the nucleotide-binding fold are likely to differ in detail. For example, the presence of several proline residues in the region corresponding to α1 of D2 suggests that this helix is substantially shortened, kinked, or split into two contiguous helices in other AAA proteins. Likewise, it appears that helix 3 may be shorter by one turn in other family members. In contrast to the nucleotide-binding fold residues 505–676, the alignment of the C-terminal helical domain of D2 with other AAA proteins, including D1, is less certain, which may indicate substantial differences in this region of the structure.

Despite the fact that many AAA proteins form hexamers, the residues that define the hexamer interface are not particularly well conserved, and there is no obvious "hexamerization signature" that defines these interfaces. Thus, the general architecture of the D2 hexamer is probably common to hexameric AAA proteins, but the details of the interprotomer interfaces are likely to vary. This would account for the different sizes of the inner hole found in images of NSF and p97 (Peters et al., 1992; Whiteheart and Kubalek, 1995; Hanson et al., 1997). Moreover, although D1 appears to form a ring of similar

(C) Ribbon diagram of D2, with AMPPNP shown in a ball-and-stick representation. To aid in following the path of the backbone, the ribbon is white at the N terminus and becomes progressively darker moving toward the C terminus. The P loop and DExx box are green and red, respectively.

(D) Ribbon diagram of the first two domains of *E. coli* DNA polymerase III δ' (Guenther et al., 1997), shown in the same orientation and color scheme as (C), except for a zinc-binding insert unique to δ' (α3), which is shown in white. (B)–(D), as well as Figures 2B and 3, were prepared with MOLSCRIPT (Kraulis, 1991).

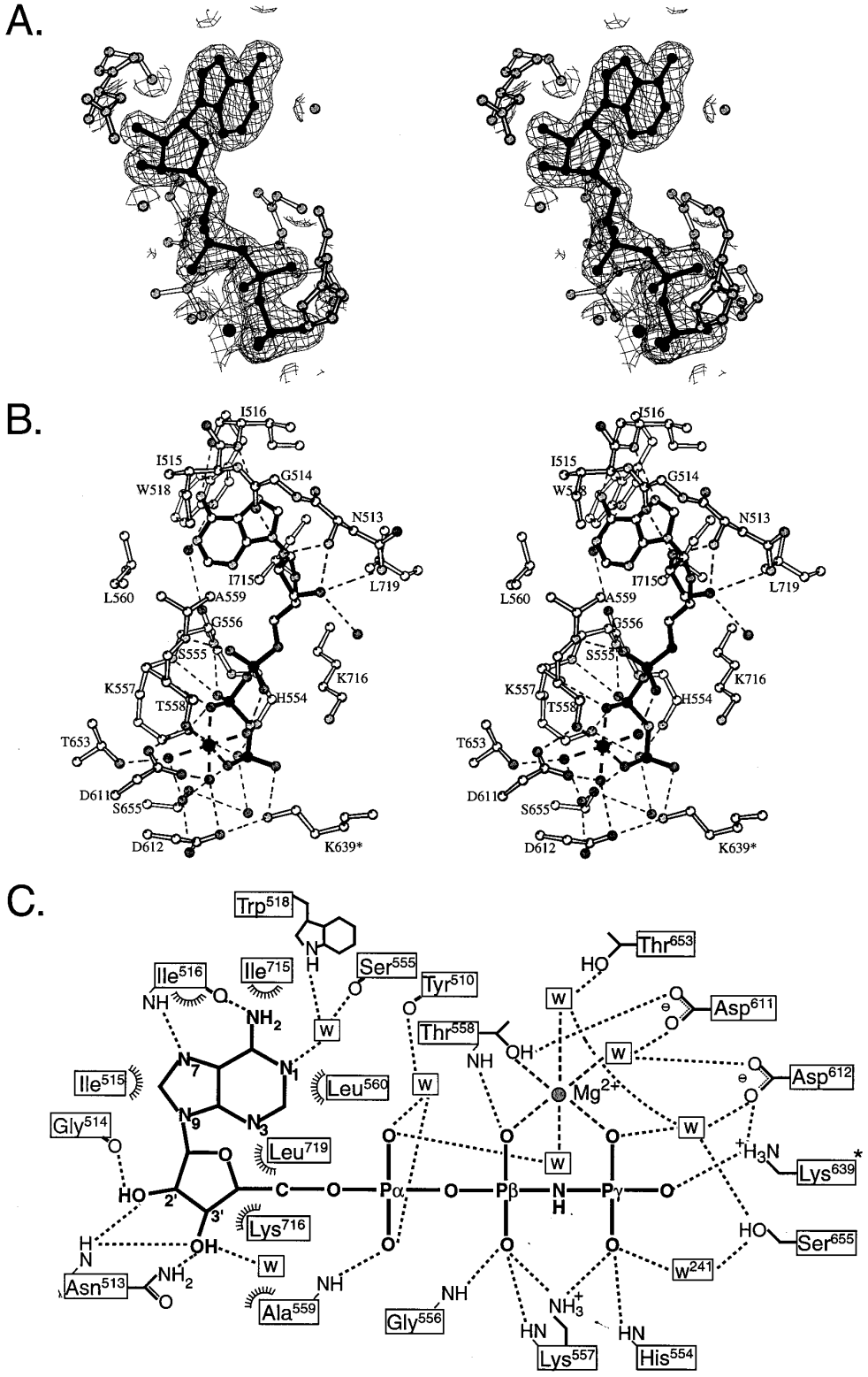

Figure 2. Nucleotide Binding by D2

(A) Stereo view of the refined $2F_o-F_c$ electron density map within 2.4 Å of AMPPNP, contoured at 1.5 σ. The refined model is shown with AMPPNP and Mg^{2+} in black, and protein and water molecules in white. The figure was prepared with BOBSCRIPT (Esnouf, 1997).

(B) Stereo view of nucleotide-binding site. AMPPNP is shown with black bonds. White, light gray, dark gray, and black spheres denote carbon, nitrogen, oxygen, and phosphorus atoms, respectively. Mg^{2+} is shown as a larger black sphere. Water molecules are shown as single oxygen atoms. Hydrogen bonds are shown as thin dashed lines; Mg^{2+} coordination bonds are shown as thick dashed lines. For clarity, the backbone at position 510 and the water molecule that interacts with the α-phosphate oxygens (see [C]) are not shown.

(C) Schematic diagram of the interactions between AMPPNP and D2. Water molecules are indicated by "W." Hydrogen and Mg^{2+} coordination bonds are indicated with dashed lines. Main-chain amide and carbonyl oxygen groups that interact with the ligand are shown emanating from the box surrounding the residue name, and side chain functionalities are shown schematically. Nonpolar van der Waals contacts are indicated by arcs. In (B) and (C), the asterisk at Lys-639 designates that this residue comes from an adjacent protomer in the D2 hexamer. This lysine appears to be only partially occupied, and its interaction with Oγ of AMPPNP is likely replaced by a water molecule in a fraction of the molecules in the crystal (see text).

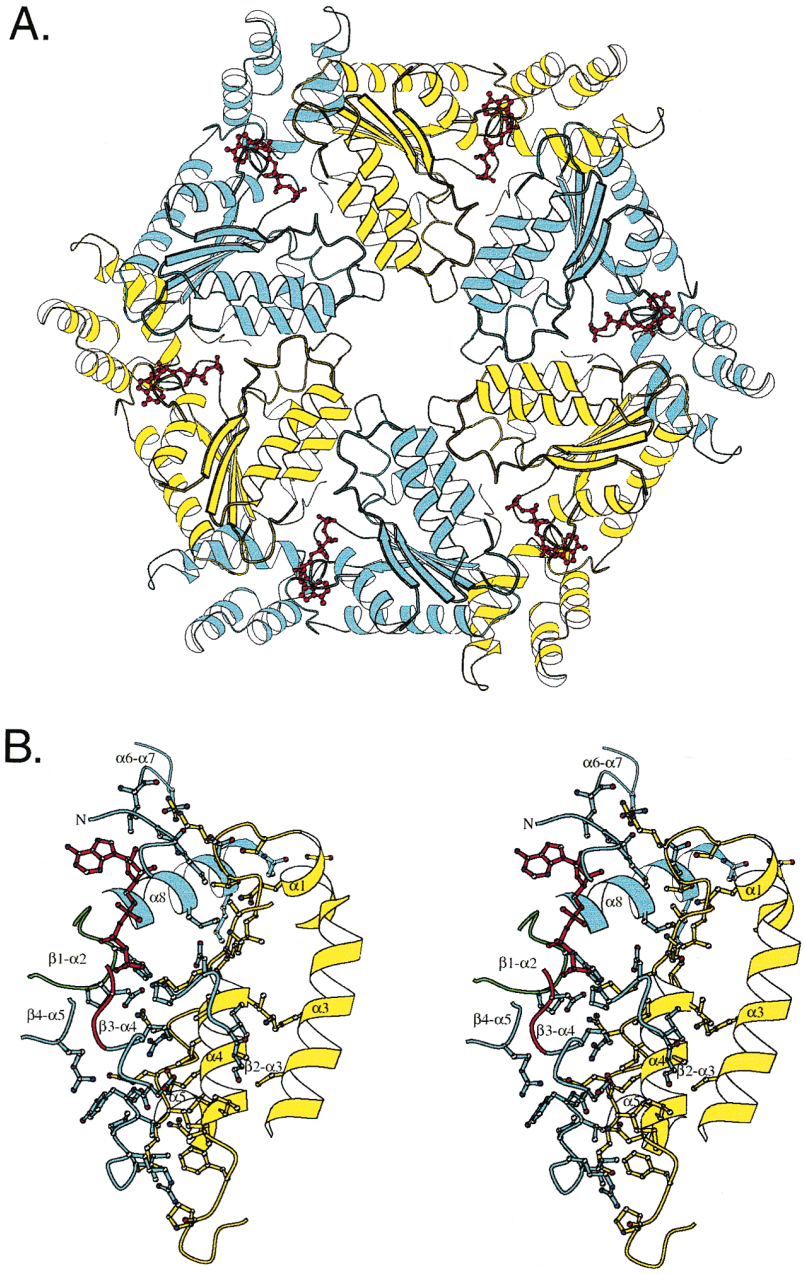

Figure 3. Structure of the D2 Hexamer

(A) Ribbon diagram of hexamer viewed down the 6-fold axis. The N-terminal side is closer to the viewer. Adjacent protomers are shown in cyan and yellow, and the bound AMPPNP is shown in red.

(B) Stereo diagram of the interface between adjacent protomers. The different protomers are shown in cyan and yellow. The backbones of the relevant regions are shown as a ribbon representation and labeled; loops in the cyan copy are labeled according to their flanking elements of secondary structure. The amino-terminal loop is labeled "N." The backbone of the P loop and DExx box of the cyan protomer are shown in green and red, respectively. Residues that form hydrogen bonds and/or van der Waals contacts across the interface are shown colored by protomer, and the AMPPNP is shown with red bonds. Water molecules in the interfaces have been omitted for clarity. White, blue, red, yellow, and magenta spheres represent carbon, nitrogen, oxygen, sulfur, and phosphorus atoms, respectively.

size to D2 in nucleotide-bound NSF, it does not oligomerize by itself (Whiteheart et al., 1994), demonstrating that there are significant differences in interprotomer interactions between D1 and D2.

NSF D2 has an extremely high affinity for adenine nucleotides, with K_d's of approximately 40 nM for ATP and 2 μM for ADP (Matveeva et al., 1997). In contrast, D1 binds to ATP and ADP with estimated K_d's of 40 μM and 140 μM, respectively (Matveeva et al., 1997). The triphosphate-binding residues are largely conserved among the AAA proteins (Figure 5), except for Thr-653, which in D2 positions a water molecule that ligates the Mg^{2+} (Figures 2B and 2C). The nucleoside-binding pocket in D2 that gives rise to the unusual *syn* conformation of the adenosine moiety also appears to be conserved. The side chains that contribute to the hydrophobic packing interactions that define the pocket are conserved in character, with the exception of Ile-516, which is often replaced with a polar residue (Figure 5). Moreover, Gly-514, whose main-chain conformation helps to define the shape of the adenine-binding pocket, is well conserved. A noteworthy feature is the presence of an alanine at position 562 in α2 that packs against Ile-511 of the N-terminal loop. This interaction appears to be conserved in Sec18p D2, but the alanine is replaced by basic residues in many other AAA proteins,

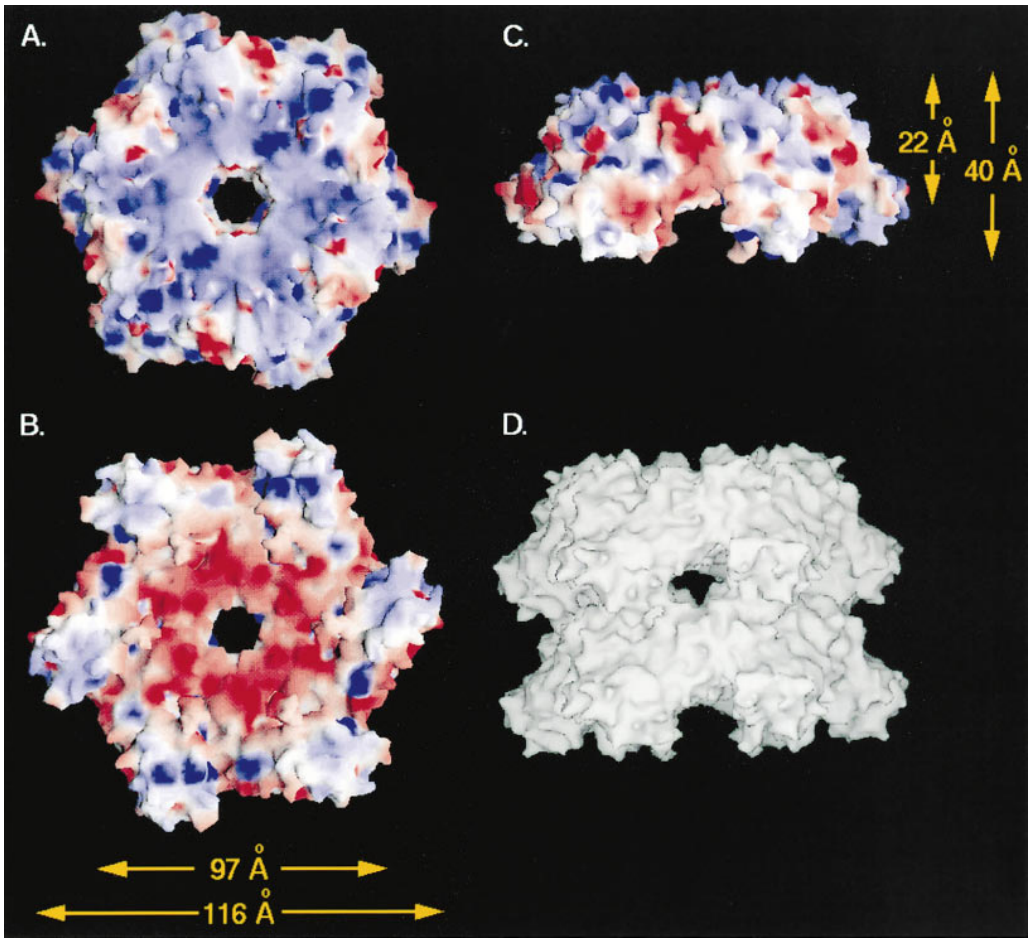

Figure 4. Surface Representation of the D2 Hexamer

In (A)–(C), blue and red represent regions of positive and negative potential, respectively, at the 10 kT/e level. The approximate dimensions are indicated.

(A) View of the N-terminal side of the hexamer; the D1 domain would be predicted to face this surface.

(B) View of the C-terminal side, rotated 180° about the horizontal with respect to the view in (A).

(C) Side view, rotated 90° about the horizontal from that in (B).

(D) Side view showing two hexamers related by a unit cell translation along the crystallographic c (6-fold) axis, correponding to the organization of D1 and D2 in full-length NSF.

including D1. It is possible that one or more of these sequence differences in or near the binding site gives rise to the high nucleotide affinity of D2.

Discussion

Nucleotide Hydrolysis

NSF D2 displays little or no ATPase activity, but its homology to D1 indicates that the interactions observed here can be used as a guide to understanding the mechanism of the catalytically active D1. It is also of interest to understand why D2 is such a poor ATPase despite the conservation of its nucleotide-binding site. To do so, the structure can be examined in light of various proposals concerning the catalytic mechanism of DExx box and other nucleoside triphosphatases. Hydrolysis requires bond formation with a water molecule and breakage of the β-γ P-O bond. In a dissociative mechanism, the bond to the leaving group is almost broken to give a metaphosphate-like transition state, whereas an associative mechanism features significant bond formation with the incoming water to give a trigonal bipyramidal transition state. In the latter case, a catalytic base must activate water for nucleophilic addition. In D2, the water molecule that interacts with Ser-655 and a γ-phosphate oxygen (wat^{241}; Figures 2B and 2C) occupies a position very similar to that of the proposed catalytic water in p21^{ras} (Pai et al., 1990), but, as in p21^{ras}, there are no acidic residues associated with it. It has been suggested that the γ-phosphate serves as the catalytic base (Schweins et al., 1995) in p21^{ras}. The glutamate of the DExx motif has also been proposed to be a catalytic base (Subramanya et al., 1996; Korolev et al., 1997), but no structures of an ATP-bound DExx-box protein have been reported. The DExx-box glutamate in D1 is essential for NSF activity (Whiteheart et al., 1994; Nagiec et al., 1995). Modeling the equivalent glutamate at position 612 of D2 does not reveal an interaction with wat^{241}, but

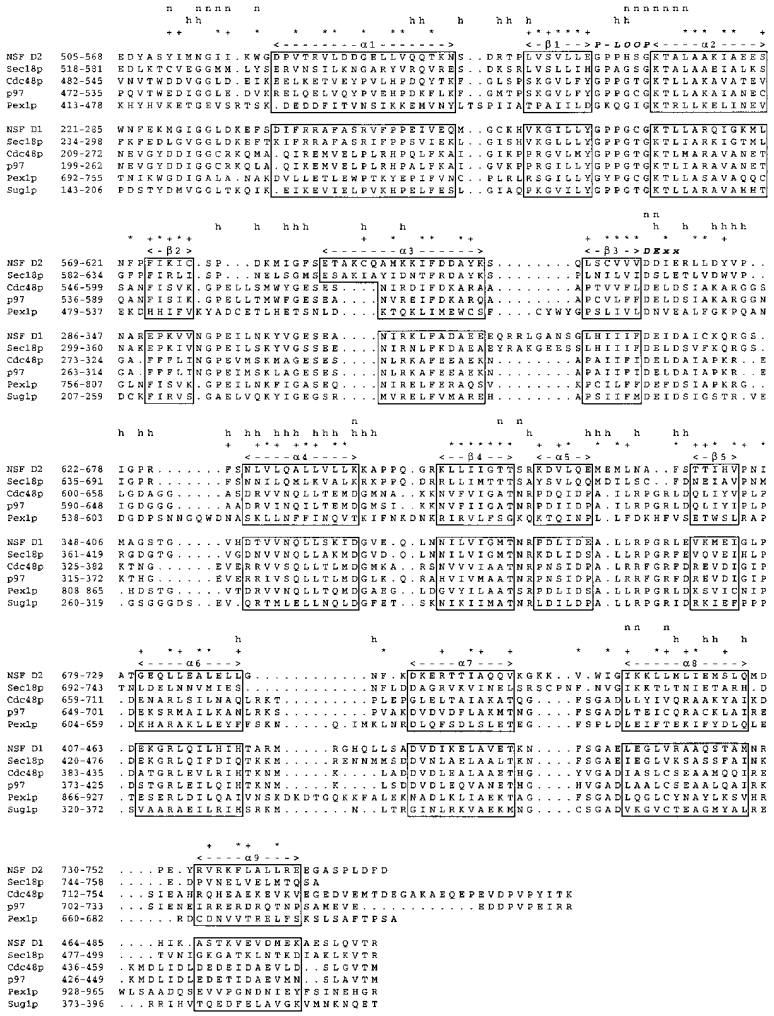

Figure 5. Structure-Based Sequence Alignment of D2 and Other AAA Domains

Representatives from several classes of AAA proteins are shown. Regions of AAA proteins corresponding to NSF D2 are shown in the upper block, and NSF D1 and its homologs are shown in the bottom block. On the line above the D2 block, elements of secondary structure are indicated. *, key buried hydrophobic positions; +, other residues that contribute to the hydrophobic core; n, residues that participate in nucleotide binding; h, residues in the hexamer interface that directly interact with residues of another protomer (based on hydrogen bond distance cutoff of 3.4 Å and van der Waals distance cutoff of 4.0 Å). The sequences and their EMBL accession numbers are NSF, Chinese hamster ovary NSF (X15652); Sec18p, the NSF ortholog of *Saccharomyces cerevisiae* (Z35949); Cdc48p from *Saccharomyces cerevisiae*, an NSF homolog involved in ER and Golgi membrane fusion and biogenesis (Z74174); p97 from *Xenopus laevis*, the ortholog of Cdc48p (X54240); Pex1p from *Saccharomyces cerevisiae*, involved in peroxisome biogenesis (Z28197); and Sug1p from *Saccharomyces cerevisiae*, a proteosome component (Z72570).

the glutamate might interact with other water molecules in the vicinity. The implicit assumption of a strictly associative transition state in models requiring a catalytic base has been questioned (Maegley et al., 1996), and the role of the DExx-box glutamate may instead be to position the attacking water molecule, perhaps through other water molecules.

Several other features of the binding site may relate to the poor activity of D2. The importance of basic residues near the phosphate oxygens, which would stabilize negative charge in an associative transition state or serve to position reactants, has been noted in G proteins (Coleman et al., 1994; Sondek et al., 1994), F1 ATPase (Abrahams et al., 1994), and many other enzymes. D2 does not share this feature, but sequence alignments do not reveal basic residues near the site in D1 and other catalytically active AAA proteins. In D2, the only basic residues near the site other than Lys-557 of the P loop are the partially occupied Lys-639 from an adjacent protomer and Lys-716 from α8, neither of which is conserved. Moreover, Lys-716 forms nonpolar interactions with the nucleotide, but its terminal amine is positioned well away from the nucleotide. Another unusual feature of D2 is the hydrogen bond between the main-chain of His-554 and a γ-phosphate oxygen (Figures 2B and 2C). In other P-loop proteins, the main-chain amide at this position interacts with the β-γ bridge oxygen. It has been proposed that this interaction has an important role in catalysis by stabilizing the negative charge that would develop at this position in a dissociative transition state (Maegley et al., 1996). In this case, the absence of this interaction may contribute to the poor catalytic rate of D2. It is also possible that the presence of NH instead of O in the β-γ phosphate bridge of AMPPNP produces this unusual interaction, but the similarity of the rest of the site to other P-loop proteins and the fact that the bridging NH lies near the backbone amide in the GMPPNP complex of p21^{ras} (Pai et al., 1990) argue against this possibility. Finally, it is not known if nucleotide hydrolysis or release is rate limiting, but it is possible that the poor catalytic rate of D2 reflects its extremely high nucleotide affinity relative to D1 (Matveeva et al., 1997).

Coupling of Nucleotide Hydrolysis and Structural Changes

To understand the mechanism by which NSF dissociates the SNAP–SNARE complex, including the role of

oligomerization, structures of the full molecule in the ATP and ADP-bound states will be required. There is no conclusive evidence that D2 can hydrolyze ATP or that the structure of ADP-bound D2 is significantly different from the ATP-bound molecule. Nonetheless, the homology of D2 to D1 and other AAA cassettes allows us to identify three regions of the structure whose conformations in D1 are likely to be sensitive to the state of the bound nucleotide, and that may be able to transmit conformational changes across the hexamer interfaces in the D1 ring or to the other domains of NSF. First, a portion of the P loop lies in the hexamer interface (Figure 3B). In other proteins, for example transducin and $G_{i\alpha}$ (Lambright et al., 1994; Mixon et al., 1995), nucleotide hydrolysis leads to significant movements of the P loop. Second, the DExx-box region lies immediately N-terminal to the long loop between β3 and α4 that forms many interprotomer contacts. The direct involvement of these residues in binding to the γ-phosphate (Figures 2B and 2C) indicates that the structure of this region might be sensitive to the state of the bound nucleotide. Third, helix α8 contributes several residues to nucleotide binding and also contains several hexamer interface residues (Figures 2B, 3B, and 5).

The participation of several residues of α8 in nucleotide binding suggests that the equivalent helix in D1 is a principal site of transmission of hydrolysis-induced conformational changes in NSF, possibly by reorientation with respect to the nucleotide-binding domain upon hydrolysis. Such movements have precedent in other ATP-binding proteins, for example adenylate kinase (Gerstein et al., 1993), and are believed to be essential elements of the coupling between ATP hydrolysis and helicase activity in DExx-box helicases (Subramanya et al., 1996; Korolev et al., 1997). A nucleotide-binding domain whose nucleotide-binding site interfaces directly to another domain permits direct coupling of nucleotide hydrolysis with structural changes and may also be important to the allosteric properties of the molecule. In G proteins, a helical domain serves to reduce the solvent accessibility of the nucleotide-binding site, allowing for regulated exchange of nucleotide by, for example, 7-helix receptors (Noel et al., 1993). Likewise, binding to the SNAP–SNARE complex appears to enhance the ATPase activity of NSF (Morgan et al., 1994; Barnard et al., 1996; Barnard et al., 1997; E. A. Matveeva and S. W. W., unpublished observations), suggesting that this interaction has effects on the structure of the nucleotide-binding site of D1.

The poor activity and the much higher affinity for ATP than for ADP displayed by D2 (Matveeva et al., 1997) suggest that in the cell D2 is principally in the ATP-bound form described here. D2 may serve to enhance the activity of D1 rather than to provide independent ATPase activity, since the activity of D1-D2 is only 1.5-fold lower than full-length NSF, whereas N-D1 is 5-fold less active (Nagiec et al., 1995). The homology of D1 and D2, as well as the presence of nucleotide-binding residues in the N-terminal loop and in α8 near the C terminus, raises the possibility that interactions between the nucleotide and the N-terminal loop of D2 help to structure the α8 region of D1 to form an active site. The importance of nucleotide binding to the formation of a well-ordered structure is suggested by the extreme sensitivity of full-length NSF to proteases in the absence of nucleotide or in the presence of ADP (Hanson et al., 1997).

Concerted action of NSF subunits triggered by ATP hydrolysis may be required to achieve disassembly of the SNAP–SNARE complex. The SNAP–SNARE complex appears to bind along the 6-fold axis of NSF (Hanson et al., 1997), suggesting that it interacts with each of the NSF protomers. Moreover, oligomers containing mixtures of active and inactive D1 domains fail to support the transport activity of NSF, suggesting that NSF requires a full complement of active D1 domains (Whiteheart et al., 1994; Nagiec et al., 1995). It is interesting that several helicases, which are likely to have a RecA-like nucleotide-binding fold (Bird et al., 1998), are homohexamers (Egelman, 1996). Like NSF, the heterohexameric mitochondrial F1 ATPase contains both active and inactive ATPase domains, the latter of which are thought to act as mechanical couplers (Abrahams et al., 1994; Boyer, 1997). The clamp loader of DNA polymerase III (Guenther et al., 1997) functions as a heterooligomer and requires active (γ) and inactive (δ') subunits. By homology to δ', helix 9 of γ (equivalent to α8 of D2) is near the ATP-binding site and has been proposed to transduce changes resulting from nucleotide hydrolysis into the conformational changes required to load the β clamp onto DNA (Guenther et al., 1997). By analogy to these examples, the D2 hexamer may mechanically couple conformational changes produced when D1 hydrolyzes ATP. Finally, the similarity of D2 to the clamp-loading ATPase, and the presence of a RecA-like core in their nucleotide-binding domains, suggests an evolutionary relationship among these oligomeric ATPases that couple ATP hydrolysis to conformational changes in substrate molecules.

Experimental Procedures

Expresssion and Purification of NSF D2

Residues 495–752 of Chinese hamster ovary NSF fused to a 14-residue amino-terminal sequence containing His_6 were expressed in *E. coli* JM109 cells and purified on Ni^{2+}-NTA agarose as described (Nagiec et al., 1995). Further purification was performed on a Superdex 200 (Pharmacia) gel filtration column run with a buffer containing 20 mM Tris-HCl (pH 8.0), 600 mM KCl, 5 mM $MgCl_2$, and 5 mM dithiothreitol (DTT). The D2 protein was concentrated in a Centricon 10 (Amicon) to a final concentration of 30 mg/ml. The protein was estimated to be greater than 95% pure by SDS-PAGE. Glycerol was added to the concentrated protein to a final concentration of 10%, and aliquots and frozen in liquid nitrogen for storage at −70°C.

Crystallization and Data Collection

Glycerol was removed from thawed protein aliquots by gel filtration on a NAP5 column (Pharmacia) in 20 mM HEPES (pH 7.5), 600 mM KCl, and the protein reconcentrated using a Centricon 10 membrane. For the crystal used in the native data set, 2 mM AMPPNP, 5 mM $MgCl_2$, 5 mM $GdCl_3$, and 2 mM DTT were added to the protein after concentration. For the derivative crystal, 5 mM $MgCl_2$ was included in the buffer used for the NAP5 column, and 10 mM AMPPNP and 2 mM DTT were added to the protein after concentration. Crystals with a hexagonal rod morphology, size $0.40 \times 0.15 \times 0.15$ mm^3, were grown in 1–2 days at 20°C by hanging drop vapor diffusion by mixing equal volumes of 20 mg/ml D2 with reservoir solutions containing 3%–8% polyethylene glycol 3350/100 mM Tris-HCl (pH 8.0). The space group is P6, with unit cell dimensions $a = 116.3$ Å, $c = 40.2$ Å.

For data collection, crystals were serially transferred through solutions containing 0%, 5%, 10%, 15%, and 20% glycerol in 16% PEG 3350, 100 mM Tris (pH 8.0), 600 mM KCl, 5 mM $MgCl_2$, 2 mM DTT, and either 2 mM AMPPNP/5 mM $GdCl_3$ (native) or 10 mM AMPPNP/1 mM ethyl mercury phosphate (EMP) over 1 hr, and flash cooled in a 100 K nitrogen stream. Data for both native and derivative crystals were measured on an RAXIS-IIc imaging plate detector mounted on a rotating copper anode. A single crystal was used for each data set. Friedel pairs for the EMP data were collected by inverse beam geometry. Data were integrated and scaled using DENZO and SCALEPACK (Otwinowski, 1993). Friedel mates were treated as independent reflections during reduction of the EMP data. Data collection and scaling statistics are shown in Table 1A.

Phasing, Model Building, and Refinement

The native and EMP data sets were highly isomorphous (Table 1A). A difference Patterson synthesis revealed a single mercury site, which was refined with MLPHARE (Collaborative Computational Project No. 4, 1994) to give a set of SIRAS phases (Table 1B). Difference Fourier maps made with these phases revealed no other sites. The phases were improved by solvent flattening and histogram matching implemented in the DM program, using the "reflection omit" mode (Cowtan and Main, 1996). The resulting 2.3 Å map was readily interpretable, and a model was built with O (Jones et al., 1991). A random 10% of the data were removed prior to refinement and constituted the test set for cross validation (Brünger, 1992). The model was refined with CNS (Brünger et al., 1998), using a maximum likelihood amplitude target (Pannu and Read, 1996), and all data with $|F| > 0$. An overall anisotropic temperature factor (Sheriff and Hendrickson, 1987) was applied throughout. Refinement consisted of two rounds of simulated annealing followed by rounds of minimization and isotropic temperature factor refinement, using a low resolution cutoff of 10 Å. After placing about 150 water molecules, a bulk solvent correction (Jiang and Brünger, 1994) was applied so that all low resolution data could be used. The side chains of eight residues have been modeled in two conformations. Refinement statistics are shown in Table 1C. The final model includes 246 amino acids, one AMPPNP, one Mg^{2+}, 271 water molecules, and one molecule of glycerol (2238 nonhydrogen atoms).

Acknowledgments

We thank D. Herschlag, A. Kolatkar, J. Kuriyan, E. Matveeva, K. Misura, and J. Wedekind for advice and discussions. C. U. L. was supported by a Deutsche Forschungsgemeinschaft Postdoctoral Fellowship. This work was supported by the National Institutes of Health (S. W. W.), the Pew Scholars Program in the Biomedical Sciences, and a Stanford University/Howard Hughes Medical Institute Junior Faculty award (W. I. W.).

Received June 22, 1998; revised July 15, 1998.

References

Abrahams, J.P., Leslie, A.G.W., Lutter, R., and Walker, J.E. (1994). Structure at 2.8 Å resolution of F1-ATPase from bovine heart mitochondria. Nature *370*, 621–628.

Banerjee, A., Barry, V.A., DasGupta, B.R., and Martin, T.F.J. (1996). N-ethylmaleimide-sensitive factor acts at a prefusion ATP-dependent step in Ca^{2+}-activated exocytosis. J. Biol. Chem. *271*, 20223–20226.

Barnard, R.J.O., Morgan, A., and Burgoyne, R.D. (1996). Domains of alpha-SNAP required for the stimulation of exocytosis and for N-ethylmaleimide-sensitive fusion protein (NSF) binding and activation. Mol. Biol. Cell *7*, 693–701.

Barnard, R.J.O., Morgan, A., and Burgoyne, R.D. (1997). Stimulation of NSF ATPase activity by α-SNAP is required for SNARE complex disassembly and exocytosis. J. Cell Biol. *139*, 875–883.

Bennett, M.K., and Scheller, R.H. (1994). A molecular description of synaptic vesicle membrane trafficking. Annu. Rev. Biochem. *63*, 63–100.

Beyer, A. (1997). Sequence analysis of the AAA protein family. Protein Sci. *6*, 2043–2058.

Bird, L.E., Subramanya, H.S., and Wigley, D.B. (1998). Helicases: a unifying structural theme? Curr. Opin. Struct. Biol. *8*, 14–18.

Block, M.R., Glick, B.S., Wilcox, C.A., Wieland, F.T., and Rothman, J.E. (1988). Purification of an N-ethylmaleimide-sensitive protein catalyzing vesicular transport. Proc. Natl. Acad. Sci. USA *85*, 7852–7856.

Boyer, P.D. (1997). The ATP synthase: a splendid molecular machine. Annu. Rev. Biochem. *66*, 717–749.

Brünger, A.T. (1992). Free R value: a novel statistical quantity for assessing the accuracy of crystal structures. Nature *355*, 472–475.

Brünger, A.T., Adams, P.D., Clore, G.M., Gros, P., Grosse-Kunstleve, R.W., Jiang, J.-S., Kuszewski, J., Nilges, M., Pannu, N.S., Read, R.J., Rice, L.M., Simonson, T., and Warren, G.L. (1998). Crystallography and NMR system (CNS): a new software system for macromolecular structure determination. Acta Crystallogr. D, in press.

Burgoyne, R.D., and Morgan, A. (1998). Analysis of regulated exocytosis in adrenal chromaffin cells: insights into NSF/SNAP/SNARE function. BioEssays *20*, 328–335.

Coleman, D.E., Berghuis, A.M., Lee, E., Linder, M.E., Gilman, A.G. and Sprang, S.R. (1994). Structures of active conformations of $G_{i\alpha1}$ and the mechanism of GTP hydrolysis. Science *265*, 1405–1412.

Collaborative Computational Project No. 4 (1994). The CCP4 suite: programs for protein crystallography. Acta Crystallogr. *D50*, 760–763.

Cowtan, K.D., and Main, P. (1996). Phase combination and cross validation in iterated density-modification calculations. Acta Crystallogr. *D52*, 43–48.

Eakle, K.A., Bernstein, M., and Emr, S.D. (1988). Characterization of a component of the yeast secretion machinery: identification of the SEC18 gene product. Mol. Cell. Biol. *8*, 4098–4109.

Egelman, E.H. (1996). Homomorphous hexameric helicases: tales from the ring cycle. Curr. Opin. Struct. Biol. *4*, 759–762.

Esnouf, R.M. (1997). An extensively modified version of MolScript that includes greatly enhanced coloring capabilities. J. Mol. Graph. *15*, 133–138.

Fleming, K.G., Hohl, T.M., Yu, R.C., Müller, S.A., Wolpensinger, B., Engel, A., Engelhardt, H., Brünger, A.T., Söllner, T.H., and Hanson, P.I. (1998). A revised model for the oligomeric state of the N-ethylmaleimide-sensitive fusion protein, NSF. J. Biol. Chem. *273*, 15675–15681.

Gerstein, M., Schulz, G., and Chothia, C. (1993). Domain closure in adenylate kinase. J. Mol. Biol. *229*, 494–501.

Graham, T.R., and Emr, S.D. (1991). Compartmental organization of Golgi-specific protein modification and vacuolar protein sorting events defined in a yeast sec18 (*NSF*) mutant. J. Cell Biol. *114*, 207–218.

Guenther, B., Onrust, R., Sali, A., O'Donnell, M., and Kuriyan, J. (1997). Crystal structure of the δ' subunit of the clamp-loader complex of *E. coli* DNA polymerase III. Cell *91*, 335–345.

Hanson, P.I., Roth, R., Morisaki, H., Jahn, R., and Heuser, J.E. (1997). Structure and conformational changes in NSF and its membrane receptor complexes visualized by quick-freeze/deep-etch electron microscopy. Cell *90*, 523–535.

Jiang, J.-S., and Brünger, A.T. (1994). Protein hydration observed by X-ray diffraction. J. Mol. Biol. *243*, 100–115.

Jones, T.A., Zou, J.-Y., Cowan, S.W., and Kjeldgaard, M. (1991). Improved methods for the building of protein models in electron density maps and the location of errors in these models. Acta Crystallogr. *A47*, 110–119.

Koonin, E.V. (1993). A common set of conserved motifs in a vast variety of putative nucleic acid-dependent ATPases including MCM proteins involved in the initiation of eukaryotic DNA replication. Nucleic Acids Res. *21*, 2541–2547.

Korolev, S., Hsieh, J., Gauss, G.H., Lohman, T.M., and Waksman, G. (1997). Major domain swiveling revealed by the crystal structures of binary and ternary complexes of *E. coli* Rep helicase bound to single-stranded DNA and ADP. Cell *90*, 635–647.

Kraulis, P.J. (1991). MOLSCRIPT: a program to produce both detailed and schematic plots of protein structures. J. Appl. Cryst. *24*, 946–950.

Lambright, D.G., Noel, J.P., Hamm, H.E., and Sigler, P.B. (1994). Structural determinants for activation of the α-subunit of a heterotrimeric G protein. Nature *369*, 621–628.

Laskowski, R.A., MacArthur, M.W., Moss, D.S., and Thornton, J.M. (1993). PROCHECK: a program to check the stereochemical quality of protein structures. J. Appl. Crystallogr. *26*, 283–291.

Linder, P., Lasko, P.F., Ashburner, M., Leroy, P., Nielsen, P.J., Nishi, K., Schnier, J., and Slonimski, P.P. (1989). Birth of the D-E-A-D box. Nature *337*, 121–122.

Maegley, K.A., Admiraal, S.J., and Herschlag, D. (1996). Ras-catalyzed hydrolysis of GTP: a new perspective from model studies. Proc. Natl. Acad. Sci. USA *93*, 8160–8166.

Matveeva, E.A., He, P., and Whiteheart, S.W. (1997). N-ethylmaleimide-sensitive fusion protein contains high and low affinity ATP-binding sites that are functionally distinct. J. Biol. Chem. *272*, 26413–26418.

Mayer, A., and Wickner, W. (1997). Docking of yeast vacuoles is catalyzed by the ras-like GTPase Ypt7p after symmetric priming by Sec18p (NSF). J. Cell Biol. *136*, 307–317.

Mayer, A., Wickner, W., and Haas, A. (1996). Sec18p (NSF)-driven release of Sec17p (α-SNAP) can precede docking and fusion of yeast vacuoles. Cell *85*, 83–94.

Mixon, M.B., Lee, E., Coleman, D.E., Berghuis, A.M., Gilman, A.G., and Sprang, S.R. (1995). Tertiary and quaternary structural changes in $G_{i\alpha 1}$/induced by GTP hydrolysis. Science *270*, 954–960.

Morgan, A. (1996). Classic clues to NSF function. Nature *382*, 680.

Morgan, A., and Burgoyne, R.D. (1995). Is NSF a fusion protein? Trends Cell Biol. *5*, 335–339.

Morgan, A., Dimaline, R., and Burgoyne, R.D. (1994). The ATPase activity of N-ethylmaleimide-sensitive fusion protein (NSF) is regulated by soluble NSF attachment proteins. J. Biol. Chem. *269*, 29347–29350.

Nagiec, E.E., Bernstein, A., and Whiteheart, S.W. (1995). Each domain of the N-ethylmaleimide-sensitive fusion protein contributes to its transport activity. J. Biol. Chem. *270*, 29182–29188.

Nichols, B.J., Ungermann, C., Pelham, H.R.B., Wickner, W.T., and Haas, A. (1997). Homotypic vacuolar fusion mediated by t- and v-SNAREs. Nature *387*, 199–202.

Noel, J.P., Hamm, H.E., and Sigler, P.B. (1993). The 2.2 Å crystal structure of transducin-α complexed with GTPγS. Nature *366*, 654–663.

Otwinowski, Z. (1993). Oscillation reduction program. In Proceedings of the CCP4 Study Weekend: Data Collection and Processing. L. Sawyer, N. Isaacs, and S. Bailey, eds. (Daresbury, U.K.: SERC Daresbury Laboratory), pp. 56–62.

Pai, E.F., Krengel, U., Petsko, G.A., Goody, R.S., Kabsch, W., and Wittinghofer, A. (1990). Refined crystal structure of the triphosphate conformation of H-*ras* p21 at 1.35 Å resolution: implications for the mechanism of GTP hydrolysis. EMBO J. *9*, 2351–2359.

Pannu, N.S., and Read, R.J. (1996). Improved structure refinement through maximum likelihood. Acta Crystallogr. *A52*, 659–668.

Patel, S., and Latterich, M. (1998). The AAA team: related ATPases with diverse functions. Trends Cell Biol. *8*, 65–71.

Peters, J.-M., Harris, J.R., Lustig, A., Müller, S., Engel, A., Volker, S., and Franke, W.W. (1992). Ubiquitous soluble Mg^{2+}-ATPase complex: a structural study. J. Mol. Biol. *223*, 557–571.

Rothman, J.E. (1994). Mechanisms of intracellular protein transport. Nature *372*, 55–63.

Schweins, T., Geyer, M., Scheffzek, K., Warshel, A., Kalbitzer, H. R. and Wittinghofer, A. (1995). Substrate-assisted catalysis as a mechanism for GTP hydrolysis of $p21^{ras}$ and other GTP-binding proteins. Nature Struct. Biol. *2*, 36–44.

Sheriff, S., and Hendrickson, W.A. (1987). Description of overall anisotropy in diffraction from macromolecular crystals. Acta Crystallogr. *A43*, 118–121.

Smith, C.A., and Rayment, I. (1996). Active site comparisons highlight structural similarities between myosin and other P-loop proteins. Biophys. J. *70*, 1590–1602.

Söllner, T., Bennett, M.K., Whiteheart, S.W., Scheller, R.H., and Rothman, J.E. (1993a). A protein assembly-disassembly pathway in vitro that may correspond to sequential steps of synaptic vesicle docking, activation, and fusion. Cell *75*, 409–418.

Söllner, T., Whiteheart, S.W., Brunner, M., Erdjument-Bromage, H., Geromanos, S., Tempst, P., and Rothman, J.E. (1993b). SNAP receptors implicated in vesicle targeting and fusion. Nature *362*, 318–324.

Sondek, J., Lambright, D.G., Noel, J.P., Hamm, H.E., and Sigler, P.B. (1994). GTPase mechanism of G proteins from the 1.7-Å crystal structure of transducin α. GDP. AlF^{4-}. Nature *372*, 276–279.

Story, R.M., Weber, I.T., and Steitz, T.A. (1992). The structure of the *E. coli recA* protein monomer and polymer. Nature *355*, 318–325.

Subramanya, H.S., Bird, L.E., Brannigan, J.A., and Wigley, D.B. (1996). Crystal structure of a DExx box DNA helicase. Nature *384*, 379–383.

Südhof, T.C. (1995). The synaptic vesicle cycle: a cascade of protein-protein interactions. Nature *375*, 645–653.

Tagaya, M., Wilson, D.W., Brunner, M., Arango, N., and Rothman, J.E. (1993). Domain structure of an N-ethylmaleimide-sensitive fusion protein involved in vesicular transport. J. Biol. Chem. *268*, 2662–2666.

Walker, J.E., Saraste, M., Runswick, M.J., and Gay, N.J. (1982). Distantly related sequences in the α- and β-subunits of ATP synthase, myosin, kinases and other ATP-requiring enzymes and a common nucleotide binding fold. EMBO J. *1*, 945–951.

Weber, T., Zemelman, B.V., McNew, J.A., Westermann, B., Gmachl, M., Parlati, F., Söllner, T.H., and Rothman, J.E. (1998). SNAREpins: minimal machinery for membrane fusion. Cell *92*, 759–772.

Whiteheart, S.W., and Kubalek, E.W. (1995). SNAPs and NSF: general members of the fusion apparatus. Trends Cell Biol. *5*, 64–68.

Whiteheart, S.W., Rossnagel, K., Buhrow, S.A., Brunner, M., Jaenicke, R., and Rothman, J.E. (1994). N-ethylmaleimide-sensitive fusion protein: a trimeric ATPase whose hydrolysis of ATP is required for membrane fusion. J. Cell. Biol. *126*, 945–954.

Wilson, D.W., Wilcox, C.A., Flynn, G.C., Chen, E., Kuang, W.-J., Henzel, W.J., Block, M.R., Ullrich, A., and Rothman, J.E. (1989). A fusion protein required for vesicle-mediated transport in both mammalian cells and yeast. Nature *339*, 355–359.

Wilson, D.W., Whiteheart, S.W., Wiedmann, M., Brunner, M., and Rothman, J.E. (1992). A multisubunit particle implicated in membrane fusion. J. Cell Biol. *117*, 531–538.

Woodman, P.G. (1997). The roles of NSF, SNAPs and SNAREs during membrane fusion. Biochim. Biophys. Acta *1357*, 155–172.

Brookhaven Protein Data Bank Accession Numbers

Coordinates and structure factors have been deposited with accession codes 1D2N and R1D2NSF, respectively.

Note Added in Proof

The structure of NSF D2 has also been reported in the following work: Yu, R.C., Hanson, P.I., John, R., and Brünger, A.T. (1998). Structure of the ATP-dependent oligomerization domain of the N-ethylmaleimide–sensitive factor complexed with ATP. Nature Struct. Biol., in press.